Growth inhibitory action of Red Trapa natans shell methanolic extract (RTNSME) in Ehrlich ascites carcinoma (EAC) cells in Swiss Albino Mice by inducing apoptosis through inactivation of NFkB

Saharia Yeasmin Asha
University of Rajshahi
Mst. Ayesha Siddika
University of Rajshahi
Mahmud Ismail
University of Rajshahi
Arifur Rahman
University of Rajshahi
Maksudul Haque
University of Science and Technology Chitagong
A. R.M. Tareq
Atomic Energy Centre
Farhadul Islam
University of Rajshahi
Syed Rashel Kabir
University of Rajshahi
Md. Abdur Rakib
mar@ru.ac.bd

University of Rajshahi

Research Article

Keywords: Trapa natans L, apoptosis, NF-kB, GC/MS, molecular docking

Posted Date: July 23rd, 2025

DOI: https://doi.org/10.21203/rs.3.rs-6950088/v1

Additional Declarations: No competing interests reported.

Abstract

Trapa natans L., commonly known as water chestnut, is a small aquatic herb belonging to the family *Trapaceae*. Its fruit is valued for both nutritional and pharmaceutical properties. This study investigates the anticancer potential of the methanolic extract of red *Trapa natans* shell (RTNSME) against Ehrlich ascites carcinoma (EAC) cells. RTNSME demonstrated significant anticancer activity, inhibiting EAC cell growth by 76.05% compared to the untreated control. Fluorescence microscopy of DAPI-stained cells revealed classic apoptotic features such as DNA fragmentation, nuclear condensation, cell shrinkage, and membrane alterations in RTNSME-treated cells. These findings were supported by RT-PCR analysis of apoptosis-related genes. RTNSME upregulated the expression of *p53* and *Bax*, while downregulating the anti-apoptotic gene *Bcl-2*. Additionally, RTNSME suppressed the activity of the nuclear factor kappa B (NF-κB), further indicating its role in promoting apoptosis. GC-MS analysis of RTNSME identified 35 phytochemical constituents, including known bioactive and anticancer compounds such as canthaxanthin, dipyridamole, and colchiceinamide. Molecular docking studies suggested that canthaxanthin exhibits the strongest binding affinity and is likely the most potent compound against EAC cells. Overall, this study demonstrates that RTNSME exerts significant anticancer effects on EAC cells, primarily through NF-κB inactivation and induction of apoptosis.

Introduction

Cancer remains one of the deadliest diseases worldwide, claiming the lives of over six million people annually (1). While both synthetic drugs and natural compounds with anticancer properties have shown promise in cancer treatment (2, 3), current chemotherapeutic agents are often expensive and associated with severe side effects. Therefore, the development of cost-effective and safer therapeutic alternatives is a critical priority in cancer research (4). Due to their lower toxicity, wide availability, and bioactivity, natural compounds are increasingly being explored for their anticancer potential (5).

Trapa natans L., commonly known as water chestnut or water caltrop, is an annual aquatic floating herb belonging to the family Trapaceae (6). It typically grows in lakes, ponds, ditches, and other stagnant water bodies, and is widely cultivated in tropical, subtropical, and temperate regions of the world (7). Two primary varieties of *Trapa natans* are recognized. Various extracts of its fruit have been reported to exhibit a broad spectrum of pharmacological properties, including antimicrobial (8), analgesic (9), anti-inflammatory (10), antidiabetic (11), antioxidant, antiulcer, and antifungal activities (12).

Previous studies have also demonstrated the anticancer potential of *Trapa natans* in several human cancer cell lines, such as human colon cancer (Colo-205), human ductal breast carcinoma (T47D), and human breast adenocarcinoma (MCF-7) cells (13). However, its anticancer activity against Ehrlich ascites carcinoma (EAC) cells has not yet been investigated.

Our earlier study revealed that the methanolic extract of red *Trapa natans* shell (RTNSME) contains a high concentration of phytochemicals and exhibits strong antioxidant activity (14). Building on these findings, the present study aims to evaluate the anti-proliferative effects of RTNSME on EAC cells and to elucidate its underlying molecular mechanisms, with a focus on apoptosis and NF-κB signaling.

Materials and Methods

Preparation of Red Trapa natans Shell Methanolic Extract (RTNSME)

Mature *Trapa natans* fruits were procured from a local market in Rajshahi, Bangladesh. The species was taxonomically authenticated by a specialist in the Department of Botany, University of Rajshahi. The red-colored fruits were thoroughly washed with distilled water to remove surface impurities. The shells were manually separated, shade-dried, and then ground into a fine powder using a mechanical grinder. The powdered shell material was stored in an airtight container at room temperature until extraction.

The extraction process followed the method described by Luqman A. Olayaki et al. (2014) (15), with slight modifications. Approximately 150 grams of the powdered shell were soaked in 500 mL of methanol and kept under continuous stirring for 24 hours at room temperature. After initial extraction, the mixture was filtered through Whatman No. 1 filter paper, and an additional 100 mL of methanol was added to the residue for re-extraction. The combined filtrates were concentrated using a rotary evaporator at 37°C to remove the solvent. The resulting dried extract (RTNSME) was stored at 4°C in a refrigerator for further use in experiments.

Animals

Swiss albino mice (6 to 8 weeks old, weighing 25 ± 4 g) were obtained from the Department of Pharmacy, Jahangirnagar University, Bangladesh. The animals were housed in standard laboratory conditions with a 12-hour light/dark cycle and maintained at room temperature with proper ventilation. Six mice were kept per cage. All animals were provided with standard laboratory chow and drinking water *ad libitum* throughout the experimental period.

Ethical Clearance

All experimental procedures involving animals were conducted in accordance with ethical guidelines and approved by the Institutional Animal, Medical Ethics, Biosafety and Biosecurity Committee (IAMEBBC) for experimentation on Animals, Humans, Microbes, and Living Natural Sources, Institute of Biological Sciences, University of Rajshahi, Bangladesh (Approval No. 117/320 (47)/IAMEBBC/IBSc).

Cell Line

Ehrlich ascites carcinoma (EAC) cells were kindly provided by the Department of Pharmacy, Jahangirnagar University, Bangladesh. All procedures involving biosafety and animal handling were conducted in compliance with the guidelines of the Institute of Biological Sciences, University of Rajshahi, Bangladesh.

Estimation of Tumor Weight

Tumor weight was estimated following the method described by (16). Experimental mice were divided into groups, each consisting of five mice. On day 0, each mouse was intraperitoneally inoculated with 1.0×10^6 EAC cells. After 24 hours, the mice were treated with RTNSME at doses of 25, 50, and 100 mg/kg body weight, respectively, for 20 consecutive days. Tumor weight was measured every 48 hours throughout the treatment period.

Cell Growth Inhibition Determination

Cell growth inhibition was assessed as previously described (17). On day 0, mice were intraperitoneally inoculated with 1×10^6 EAC cells. After 24 hours, RTNSME was administered at doses of 25, 50, and 100 mg/kg body weight per mouse per day to the respective treatment groups for five consecutive days. A control group received only normal saline. On day 6, all animals were sacrificed, and the ascitic fluid was collected. EAC cells were harvested and counted using a hemocytometer to evaluate the extent of cell growth inhibition.

DAPI Staining for Morphological Appearance and Nuclear Damage of EAC Cells

The induction of apoptosis in EAC cells was assessed as previously described (18). Both treated and untreated control EAC cells were analyzed using a fluorescence inverted microscope (Olympus IX71, Japan). Initially, the cells were collected and stained with 25 µL of DAPI solution (1 mg/mL) at 37°C for 20 minutes. After staining, the cells were washed three times with PBS in the dark to remove excess dye. Morphological changes, including nuclear condensation and fragmentation, were observed under the fluorescence microscope to assess nuclear damage and apoptotic characteristics.

Reverse Transcriptase Polymerase Chain Reaction (RT-PCR)

Total RNA was extracted from cells using an RNA extraction kit according to the manufacturer's instructions. cDNA was synthesized via reverse transcription PCR following the protocol provided with the kit. The primers used for the experiment are listed in Table 1. The PCR products were subjected to electrophoresis on a 1.0% agarose gel, which was then stained with ethidium bromide. The gel was visualized under a UV transilluminator to assess the amplification of target genes.

Table 1
The sequence of primers used for PCR amplification.

Gene name	Primer sequence references
GAPDH	Forward: (5'-GTGGAAGGACTCATGACCACAG-3')
	Reverse: (5'-CTGGTGCTCAGTGTAGCCCAG-3')
p53	Forward: (5'-CACAAAAACAGGTTAAACCCAG-3')
	Reverse: (5'-AGCACATAGGAGGCAGAGAC-3')
Bcl-2	Forward: (5'-GTGGAGGAGCTCTTCAGGGA-3')
	Reverse: (5'-AGGCACCCAGGGTGATGCAA-3')
Bax	Forward: (5'-GGCCCACCAGCTCTGAGCAGA-3')
	Reverse: (3'-GCCACGTGGGCGTCCCAAAGT-5')
NF-kB	Forward: (5'-AACAAAATGCCCCACGGTTA-3')
	Reverse: (3'-GGGACGATGCAATGGACTGT-5')

Gas Chromatography-Mass Spectrometry (GC-MS) Analysis

GC-MS analysis of RTNSME was performed using a Varian GC spectrophotometer (Model CP-3800, USA) coupled with a Varian Saturn-2200 mass spectrometer. The system was equipped with a flame ionization detector and a VF-5 ms capillary column (30 m × 0.25 mm, 0.25 µm). The instrument was operated in electron impact mode at 70 eV ionization voltage, with the injector temperature set at 250°C and the detector temperature set at 280°C. A 1 µL sample was injected with helium as the carrier gas at a flow rate of 1 mL/min. The column temperature was initially set to 40°C for 1 minute, then ramped to 310°C at a rate of 10°C/min, where it was held for 10 minutes. Chemical compounds were identified and quantified by comparing their mass spectra with the NIST 05 Library database.

Molecular Docking Simulation

Molecular docking simulations were performed to explore the potential interactions between BAX, BCL2, p53, and NF-κB proteins with the compounds Canthaxanthin, Colchiceinamide, and Dipyridamole. The 3D structures of BAX, BCL2, p53, and NF-κB proteins were retrieved from the Protein Data Bank (PDB) (https://www.rcsb.org/) with the following PDB codes: 5W62 (BAX), 2KUA (BCL2), 2IOI (p53), and 1MY5 (NF-κB). To eliminate potential interference from water molecules and heteroatoms, these were removed using Biovia Discovery Studio 2021, reducing the possibility of undesired interactions with the receptor proteins. The resulting PDB files were then converted into pdbqt format for docking analysis.

The chemical structures of Canthaxanthin (CID: 5281227), Colchiceinamide (CID: 18397), and Dipyridamole (CID: 3108) were downloaded in 3D SDF format from the PubChem database (https://pubchem.ncbi.nlm.nih.gov/), minimized, and converted into pdbqt format using the PyRx tool. Docking studies were carried out using PyRx with Autodock Vina to predict the binding affinity and interaction between the proteins and compounds. The protein-ligand interactions, including hydrogen bonds, pi-alkyl bonds, hydrophobic interactions, and other relevant bonding types, were analyzed and visualized using BIOVIA Discovery Studio 2021.

Statistical Analysis

Experiments were performed in triplicates, and the data are presented as the mean ± standard deviation (SD). Statistical analysis was conducted using one-way analysis of variance (ANOVA), followed by Duncan's multiple range test to compare group means. All analyses were performed using SPSS software (version 16). A p-value of < 0.05 was considered statistically significant.

Results

Growth inhibition of EAC cell treated with RTNSME

Tumor weight reduction

EAC cells growth inhibition was first determined by average tumor weight. RTNSME reduced tumor weight in EAC-bearing mice significantly. Tumor weight of untreated control EAC cells was increased over time but treatment with RTNSME at the concentration of 25, 50 and 100 mg/kg RTNSME significant reduced of tumor weight (Fig. 1A).

Cell growth inhibition

Treatment with RTNSME resulted in 26.21, 38.15 and 76.05% of cell growth inhibition compared to control at 25, 50 and 100 mg/kg body weight doses respectively. Effects of RTNSME on cell growth inhibition are shown in Table 2 and Fig. 1B.

Table 2
Cell growth inhibition

Name of the experiment	Nature of Drug	Dose in mg/kg/day body weight (i.p)	No of EAC cells in mouse on Day 6 after tumour cell inoculation	% of cell growth inhibition
	Control(EAC cell bearing mice)	-	$(2.46 \pm .12) \times 10^{6\,d}$	-
	RTNSME	25	$(1.81 \pm .12) \times 10^{6\,c}$	26.21
		50	$(1.52 \pm .12) \times 10^{6\,b}$	38.15
		100	$(0.59 \pm .20) \times 10^{6\,a}$	76.05

Effect of RTNSME on EAC cell growth inhibition (*in vivo*). Data were expressed as mean ± SD (n = 3). Mean with different lowercase letters are significantly different at $P < 0.05$ by Duncan's multiple-range test.

Induction of cancer cell apoptosis

Changes of EAC cell morphology

RTNSME treated EAC cells showed condensed and fragmented DNA in nuclei as shown in Fig. 2A whereas Morphological changes of EAC untreated cells were found round, regular in control cell whereas.

Modulation of apoptotic gene expression

The mRNA expressions of p53, Bcl-2, Bax were investigated by using specific primers. Red TNSME was down regulated the mRNA expression of Bcl-2 when compared with untreated control. On the other hand, the mRNA expression of Bax, p53 was up regulated when treated with RTNSME. GAPDH expression was observed equally both in RTNSME treated EAC cells and untreated control EAC cells Fig. 2B.

Inactivation of NF-κB gene expression

NF-κB gene in EAC cells treated with RTNSME was determined by RT-PCR Fig. 3. RTNSME reduced the activation of NF-κB compared to untreated control cells. This results might reduce cell growth and induction of apoptosis.

Chemical composition of RTNSME

GC/MS chromatogram and list of compounds revealed that RTNSME consists of 35 compounds as shown in Table 3 and Fig. 4 respectively.

Table 3
Chemical composition of RTNSME analyzed by GC

SL	Compound Name	MW	Formula	RT	Area %
1	Benzyloxy(butyl)dimethylsilane	222	C13H22OSi	5.46	1.4
2	Isobutyl ether	130	C8H18O	6.06	6.16
3	1-(Nitromethyl)-cyclohexanol	159	C7H13NO3	5.26	2.26
4	Ethanol, 2-butoxy-	118	C6H14O2	6.39	2.50
5	1,2,3-Propanetriol, monoacetate	134	C5H10O4	8.14	1.65
6	Benzyl Alcohol	108	C7H8O	8.48	1.50
7	1,1,2-Triacetoxyethane	204	C8H12O6	8.57	3.81
8	Cyclopentasiloxane, decamethyl-	370	C10H30O5Si5	14.77	0.43
9	Cyclohexasiloxane, dodecamethyl-	444	C12H36O6Si6	17.33	0.95
10	Cyclooctasiloxane, hexadecamethyl-	592	C16H48O8Si8	18.13	3.44
11	Cycloheptasiloxane, tetradecamethyl-	518	C14H42O7Si7	19.59	0.82
12	4-Pyrimidinamine, 5-methyl-N-(trimethylsilyl)-2-[(trimethylsilyl)oxy]-	269	C11H23N3OSi2	20.47	5.04
13	Octadecamethyl-Cyclononasiloxane	666	C18H54O9Si9	20.60	6.53
14	Cyclodecasiloxane, eicosamethyl-	740	C20H60O10Si10	22.95	4.03
15	gamma.-Lumicolchicine	399	C22H25NO6	49.71	2.07
15	3,9.beta.;14,15-Diepoxypregn-16-en-20-one, 3,11.beta.,18-triacetoxy-	502	C27H34O9	50.05	4.03
16	2-Butenoic acid, 2-methyl-, 1,1a,1b,4,4a,5,7a,7b,8,9-decahydro-4a,7b-dihydroxy-3-(hydroxymethyl)-1,1,6,8-tetramethyl-5-oxo-9aH-cyclopropa[3,4]benz[1,2-e]azulene-9,9a-diyl ester, [1aR-[1a.alpha.,1b.beta.,4a.beta.,7a.alpha.,7b.alpha.,8.alpha.,9.beta.(E),9a.alpha.(E)]]-	528	C30H40O8	50.35	1.00
17	psi.,.psi.-Carotene, 3,4-didehydro-1,2,7',8'-tetrahydro-1-methoxy-2-oxo-	582	C41H58O2	50.52	4.17
18	9-Desoxo-9-x-acetoxy-3,8,12-tri-O-acetylingol	536	C28H40O10	51.52	2.6
19	Canthaxanthin	564	C40H52O2	51.67	5.38
20	Colchiceinamide	384	C21H24N2O5	51.76	2.67
21	Norcodeine di-TMS derivative	429	C23H35NO3Si2	51.86	3.64
22	2,4-Imidazolidinedione, 5-[3,4-bis[(trimethylsilyl)oxy]phenyl]-3-methyl-5-phenyl-1-(trimethylsilyl)	516	C25H40N2O4Si3	51.90	2.09
23	3,8,12-Triacetylingol 7-(4-methoxyphenyl)acetate	640	C35H44O11	51.97	1.52
24	6,6'-Diacetyl-7,7'-dihydroxy-2,2',4,4',5,5'-hexamethoxy-1,1'-binaphthalene	550	C30H30O10	52.08	3.95
25	D-Glucopyranosiduronic acid, 3-(5-ethylhexahydro-1,3-dimethyl-2,4,6-trioxo-5-pyrimidinyl)-1-methylbutyl 2,3,4-tris-O-(trimethylsilyl)-, methyl ester	676	C29H56N2O10Si3	52.26	3.72
26	Pregnane-11,20-dione, 3,17,21-tris[(trimethylsilyl)oxy]-, 20-[O-(phenylmethyl)oxime], (3.alpha.,5.alpha.)-	685	C37H63NO5Si3	52.35	2.24
27	Cephalotaxine, 11-(acetyloxy)-, acetate (ester), (11.alpha.)-	415	C22H25NO7	52.41	1.97
28	Silane, [[(3.beta.,5.alpha.,11.beta.,20S)-pregnane-3,11,17,20,21-pentayl]pentakis(oxy)]pentakis[trimethyl-	728	C36H76O5Si5	52.52	1.90
29	5H-Cyclopropa[3,4]benz[1,2-e]azulen-5-one, 2,4a,9,9a-tetrakis(acetyloxy)-3,[(acetyloxy)methyl]-1,1a,1b,2,3,4,4a,7a,7b,8,9,9a-dodecahydro-2,7b-dihydroxy-1,1,6,8-tetramethyl-, [1aR-(1a.alpha.,1b.beta.,2.alpha.,3.beta.,4a.beta.,7a.alpha.,7b.alpha.,8.alpha.,9.beta.,9a.alpha.)]-	608	C30H40O13	52.70	0.77
30	Dipyridamole	504	C24H40N8O4	52.82	0.70
31	6-Fluorobenzofurazane, 5-[4-(3-methoxyphenyl)piperazin-1-yl]-, 1-oxide	344	C17H17FN4O3	55.45	0.86
32	1-(3-Cyano-6-methyl-4,5,6,7-tetrahydro-thieno[2,3-c]pyridin-2-yl)-3-phenyl-thiourea	328	C16H16N4S2	57.04	0.35

SL	Compound Name	MW	Formula	RT	Area %
33	Morphinan-6-ol, 4,5-epoxy-3-methoxy-17-methyl-, acetate (ester), (5.alpha.,6.alpha.)-	343	C20H25NO4	61.02	1.35
34	Echinenone	550	C40H54O	61.50	0.43
35	2,2'-Binaphthalene]-8,8'-dicarbonitrile, 1,1'-dihydroxy-6,6',7,7'-tetramethoxy-3,3'-dimethyl-5,5'-bis(1-methylethyl)-	568	C34H36N2O6	61.87	0.80

Molecular docking simulation

Among the three compounds, no significant binding of Dipyridamole with Bax, Bcl2, p53 and NF-κB was observed as shown in Table 4. Although a significant binding of Colchiceinamide was found only with Bcl2 with the binding energy of -7.5 kcal/mol (Fig. 5A). Where Colchiceinamide formed two hydrogen bonds with residues ASN180 and SER81. Besides the hydrogen bonds, other types of bonding were also observed (Fig. 5A). But Canthaxanthin exert strong binding affinity with Bax, Bcl2, p53 and NF-κB proteins with the binding energy of -7.8, -8.6, -7.0 and − 7.0 kcal/mol, respectively (Table 4). No hydrogen bonding was observed for Bax and Bcl2 (Fig. 5B **and C**). But a strong hydrogen bonding was observed for NF-kB (Fig. 5D) and p53 (Fig. 5E). Besides hydrogen bonding other type of interaction was also observed for each of the proteins as shown in the 2D picture (Fig. 5).

Table 4
Binding energy

Protein Name	Compound Name	Binding energy (kcal/mol)
Bax	Canthaxanthin	-7.8
Bax	Colchiceinamide	-6.0
Bax	Dipyridamole	-5.4
Bcl2	Canthaxanthin	-8.6
Bcl2	Colchiceinamide	-7.5
Bcl2	Dipyridamole	-6.0
p53	Canthaxanthin	-7.0
p53	Colchiceinamide	-5.9
p53	Dipyridamole	-5.4
NFκB	Canthaxanthin	-7.0
NFκB	Colchiceinamide	-5.6
NFκB	Dipyridamole	-5.4

Discussion

The primary objective of this study was to evaluate the growth-inhibitory and anti-proliferative effects of RTNSME in Ehrlich ascites carcinoma (EAC) cells. The findings of this study provide clear evidence that RTNSME possesses significant anticancer activity, primarily by inducing apoptosis. As demonstrated in Fig. 1, RTNSME exhibited a dose-dependent growth inhibitory effect. Furthermore, DAPI staining of untreated EAC cells and RTNSME-treated cells revealed morphological alterations indicative of apoptosis, including membrane blebbing, cell shrinkage, and nuclear condensation (Fig. 2A). These results suggest that RTNSME effectively inhibits cell growth by triggering apoptotic processes.

Our previous study also reported apoptosis induction by MOLME in EAC cells (19). The Bcl-2 family of proteins plays a critical role in regulating cell cycle arrest and cell death (20), with Bcl-2 promoting cell survival (21). In contrast, p53 modulates apoptosis by binding to Bcl-2 family proteins, allowing Bax to be released and signal the mitochondria to initiate cell death (22, 23). The present study suggests that RTNSME up-regulates p53, which in turn down-regulates Bcl-2 and up-regulates Bax. As a result, the Bcl-2/Bax ratio decreases, promoting apoptotic cell death (Fig. 2B).

NF-κB is a key regulator involved in cell growth, survival, and apoptosis induction (24, 25). In cancer, NF-κB is typically up-regulated, promoting inflammation and facilitating tumorigenesis (26), while also driving metastasis (27). Activation of NF-κB generally inhibits p53 function (28, 29), meaning that p53 and NF-κB often exhibit opposing effects in cancer cells (30). In this study, we found that RTNSME inhibited NF-κB activation (Fig. 3) in conjunction with growth inhibition, suggesting that NF-κB inactivation could initiate apoptotic pathways and contribute to EAC cell death.

GC-MS analysis of RTNSME identified 35 compounds, many of which are known to possess biological activity. Notably, Canthaxanthin, a compound found in RTNSME, has been reported to act as an anti-tumor agent (31–34). Previous studies have demonstrated that Canthaxanthin inhibits the growth of murine melanoma, fibrosarcoma, and human squamous carcinoma cells in vitro (35) and can reduce cell growth by inducing apoptosis (36). Dipyridamole, also present in RTNSME, has shown antitumor activity and can enhance the sensitivity of several chemotherapy agents, including 5-fluorouracil, cisplatin, and methotrexate (37). It has also been shown to increase the sensitivity of trametinib in cancer cell lines (38). Additionally, Colchicine, an alkaloid found in RTNSME, has demonstrated anticancer potential across various cancer cell lines (39).

Molecular docking, a critical tool in computational drug design, was employed in this study to investigate the interaction between RTNSME compounds and key apoptosis-regulating proteins (Bax, Bcl-2, p53, and NF-κB). Our docking results revealed a strong binding affinity between Canthaxanthin and these proteins, supporting the activation of apoptotic pathways via the modulation of these key regulatory proteins.

Conclusion

In conclusion, RTNSME significantly inhibited EAC cell growth by inducing apoptosis. This growth inhibitory effect is likely mediated through mitochondrial dysfunction, with reciprocal changes in the expression of Bax and Bcl-2. Furthermore, inactivation of NF-κB and up-regulation of p53 appear to play central roles in promoting EAC cell death. Our findings suggest that RTNSME down-regulates NF-κB, which in turn up-regulates p53, leading to apoptosis in EAC cells.

Declarations

Funding

No specific fund provided for this study. Department of Biochemistry and Molecular Biology, University of Rajshahi, supported the study in partial.

Author Contribution

S.Y.A., M.A.S. design the study, performed the experiments and drafted the manuscript. M.I., A.R., M.H. analyzed the data and generated figures and tables, A.R.M.T. performed GC-MS, S.R.K. supported docking experiments, M.A.R., F.I. planned, supervised the project and edited the manuscript.

References

1. Abdullaev FI, Rivera-Luna R, Roitenburd-Belacortu V, Espinosa-Aguirre J. Pattern of childhood cancer mortality in Mexico. Arch Med Res. 2000;31(5):526–31. 10.1016/s0188-4409(00)00094-1.
2. Islam F, Gopalan V, Lam AKY, Kabir SR. Kaempferia rotunda tuberous rhizome lectin induces apoptosis and growth inhibition of colon cancer cells in vitro. Int J Biol Macromol. 2019;141:775–82. 10.1016/j.ijbiomac.2019.09.051.
3. Das PK, Rakib MA, Khanam JA, Pillai S, Islam F. Novel Therapeutics Against Breast Cancer Stem Cells by Targeting Surface Markers and Signaling Pathways. Curr Stem Cell Res Ther. 2019;14(8):669–82. 10.2174/1574888X14666190628104721.
4. Khatun M, Habib MR, Rabbi MA, et al. Antioxidant, cytotoxic and antineoplastic effects of Carissa carandas Linn. leaves. Exp Toxicol Pathol. 2017;69(7):469–76. 10.1016/j.etp.2017.03.008.
5. Islam F, Khatun H, Khatun M, Ali SM, Khanam JA. Growth inhibition and apoptosis of Ehrlich ascites carcinoma cells by the methanol extract of Eucalyptus camaldulensis. Pharm Biol. 2014;52(3):281–90. 10.3109/13880209.2013.834365.
6. Institute of Botany, the Chinese Academy of Sciences. Iconographia Cormophytorum Sinicorum (Tomus). Volume 52. Beijing, China: Science; 2004. p. 167.
7. Faruk MO, Amin MZ, Sana NK, Shaha RK, Biswas KK. Biochemical analysis of two varieties of water chestnuts (Trapa sp). Pak J Biol Sci. 2012;15(21):1019–26. 10.3923/pjbs.2012.1019.1026.
8. Parekh J, Chanda S. In vitro antimicrobial activity of Trapa natans L. fruit rind extracted in different solvents. Afr J Biotechnol. 2007;6(6):766–70.
9. International Journal of Natural and Social Sciences. 2020, 7(2): 77–87.
10. Patel S, Banji D, Ba nji OJF, Patel MM, Shah K. K. Scrutinizing the role of aqueous extract of Trapa bispinosa as an immunomodulator in experimental animals. Int J Res Pharm Sci. 2010;1(1):13–9.
11. Huang HC, Chao CL, Liaw CC, et al. Hypoglycemic Constituents Isolated from Trapa natans L. Pericarps. J Agric Food Chem. 2016;64(19):3794–803. 10.1021/acs.jafc.6b01208.
12. Chandana M, Mazumder R, Chakraborthy GS. A review on potential of plants under Trapa species. Int J Res Pharm Chem. 2013;3(2):502–8.

13. Gani A, Rasool N, Shah A, Ahmad M, Gani A, Wani TA, Masoodi FA. DNA scission inhibition, antioxidant, and antiproliferative activities of water chestnut (*Trapa natans*) extracted in different solvents. CyTA - J Food. 2015;13(3):415–9. https://doi.org/10.1080/19476337.2014.992967.
14. Asha SH, Siddika A, Das PK, Ismail M, Islam F, Rakib MA. Phytochemical profiling and antioxidant activity of different varieties of Trapa natans: A comparative analysis. J Pharmacognosy Phytochemistry. 2024;13(5):232–7. https://doi.org/10.22271/phyto.2024.v13.i5c.15076.
15. Olayaki LA, Irekpita JE, Yakubu MT, Ojo OO. Methanolic extract of Moringa oleifera leaves improves glucose tolerance, glycogen synthesis and lipid metabolism in alloxan-induced diabetic rats. J Basic Clin Physiol Pharmacol. 2015;26(6):585–93. 10.1515/jbcpp-2014-0129.
16. Perveen R, Islam F, Khanum J, Yeasmin T. Preventive effect of ethanol extract of Alpinia calcarata Rosc on Ehrlich's ascitic carcinoma cell induced malignant ascites in mice. Asian Pac J Trop Med. 2012;5(2):121–5. 10.1016/S1995-7645(12)60009-1.
17. Syed Abdul Rahman SN, Abdul Wahab N, Abd Malek SN. In Vitro Morphological Assessment of Apoptosis Induced by Antiproliferative Constituents from the Rhizomes of Curcuma zedoaria. Evid Based Complement Alternat Med. 2013;2013:257108. 10.1155/2013/257108.
18. Rakib MA, Kim YS, Jang WJ, Jang JS, Kang SJ, Ha YL. Preventive effect of t,t-conjugated linoleic acid on 12-O-tetradecanoylphorbol-13-acetate-induced inhibition of gap junctional intercellular communication in human mammary epithelial MCF-10A cells. J Agric Food Chem. 2011;59(8):4164–70. 10.1021/jf1046909.
19. Das PK, Asha SY, Siddika MA, Siddika A, Tareq ARM, Islam F, Khanam JA, Rakib MA. Methanolic extract of Moringa oleifera leaves mediates anticancer activities through inhibiting NF-□B and enhancing ROS in Ehrlich ascites carcinoma cells in mice. J Adv Biotechnol Exp Ther. 2021;4(2):161–70. https://doi.org/10.5455/jabet.2021.d116.
20. Zinkel S, Gross A, Yang E. BCL2 family in DNA damage and cell cycle control. Cell Death Differ. 2006;13(8):1351–9. 10.1038/sj.cdd.4401987.
21. Islam MA, Kim YS, Jang WJ, et al. A mixture of trans, trans conjugated linoleic acid induces apoptosis in MCF-7 human breast cancer cells with reciprocal expression of Bax and Bcl-2. J Agric Food Chem. 2008;56(14):5970–6. 10.1021/jf8004977.
22. Chen J. The Cell-Cycle Arrest and Apoptotic Functions of p53 in Tumor Initiation and Progression. *Cold Spring Harb Perspect Med*. 2016;6(3):a026104. Published 2016 Mar 1. 10.1101/cshperspect.a026104
23. Pellegata NS, Antoniono RJ, Redpath JL, Stanbridge EJ. DNA damage and p53-mediated cell cycle arrest: a reevaluation. Proc Natl Acad Sci U S A. 1996;93(26):15209–14. 10.1073/pnas.93.26.15209.
24. Meyer C, Sims AH, Morgan K, et al. Transcript and protein profiling identifies signaling, growth arrest, apoptosis, and NF-κB survival signatures following GNRH receptor activation. Endocr Relat Cancer. 2013;20(1):123–36. 10.1530/ERC-12-0192. Published 2013 Feb 18.
25. Alonso F, Krattinger N, Mazzolai L, et al. An angiotensin II- and NF-kappaB-dependent mechanism increases connexin 43 in murine arteries targeted by renin-dependent hypertension. Cardiovasc Res. 2010;87(1):166–76. 10.1093/cvr/cvq031.
26. Baud V, Karin M. Is NF-kappaB a good target for cancer therapy? Hopes and pitfalls. Nat Rev Drug Discov. 2009;8(1):33–40. 10.1038/nrd2781.
27. Xia Y, Shen S, Verma IM. NF-κB, an active player in human cancers. Cancer Immunol Res. 2014;2(9):823–30. 10.1158/2326-6066.CIR-14-0112.
28. Dey A, Tergaonkar V, Lane DP. Double-edged swords as cancer therapeutics: simultaneously targeting p53 and NF-kappaB pathways. Nat Rev Drug Discov. 2008;7(12):1031–40. 10.1038/nrd2759.
29. Ak P, Levine AJ. p53 and NF-κB: different strategies for responding to stress lead to a functional antagonism. FASEB J. 2010;24(10):3643–52. 10.1096/fj.10-160549.
30. Carrà G, Lingua MF, Maffeo B, Taulli R, Morotti A. P53 vs NF-κB: the role of nuclear factor-kappa B in the regulation of p53 activity and vice versa. Cell Mol Life Sci. 2020;77(22):4449–58. 10.1007/s00018-020-03524-9.
31. Tanaka T, Makita H, Ohnishi M, Mori H, Satoh K, Hara A. Chemoprevention of rat oral carcinogenesis by naturally occurring xanthophylls, astaxanthin and canthaxanthin. Cancer Res. 1995;55(18):4059–64.
32. Tanaka T, Kawamori T, Ohnishi M, et al. Suppression of azoxymethane-induced rat colon carcinogenesis by dietary administration of naturally occurring xanthophylls astaxanthin and canthaxanthin during the postinitiation phase. Carcinogenesis. 1995;16(12):2957–63. 10.1093/carcin/16.12.2957.
33. Grubbs CJ, Eto I, Juliana MM, Whitaker LM. Effect of canthaxanthin on chemically induced mammary carcinogenesis. Oncology. 1991;48(3):239–45. 10.1159/000226935.
34. Katsumura N, Okuno M, Onogi N, Moriwaki H, Muto Y, Kojima S. Suppression of mouse skin papilloma by canthaxanthin and beta-carotene in vivo: possibility of the regression of tumorigenesis by carotenoids without conversion to retinoic acid. Nutr Cancer. 1996;26(2):203–8. 10.1080/01635589609514476.
35. Huang DS, Odeleye OE, Watson RR. Inhibitory effects of canthaxanthin on in vitro growth of murine tumor cells. Cancer Lett. 1992;65(3):209–13. 10.1016/0304-3835(92)90233-I.
36. Palozza P, Maggiano N, Calviello G, et al. Canthaxanthin induces apoptosis in human cancer cell lines. Carcinogenesis. 1998;19(2):373–6. 10.1093/carcin/19.2.373.

37. Ge SM, Zhan DL, Zhang SH, Song LQ, Han WW. Reverse screening approach to identify potential anti-cancer targets of dipyridamole. Am J Transl Res. 2016;8(12):5187–98. Published 2016 Dec 15.
38. Zhou S, Xu H, Tang Q, Xia H, Bi F. Dipyridamole Enhances the Cytotoxicities of Trametinib against Colon Cancer Cells through Combined Targeting of HMGCS1 and MEK Pathway. Mol Cancer Ther. 2020;19(1):135–46. 10.1158/1535-7163.MCT-19-0413.
39. Kumar A, Sharma PR, Mondhe DM. Potential anticancer role of colchicine-based derivatives: an overview. Anticancer Drugs. 2017;28(3):250–62. 10.1097/CAD.0000000000000464.

Figures

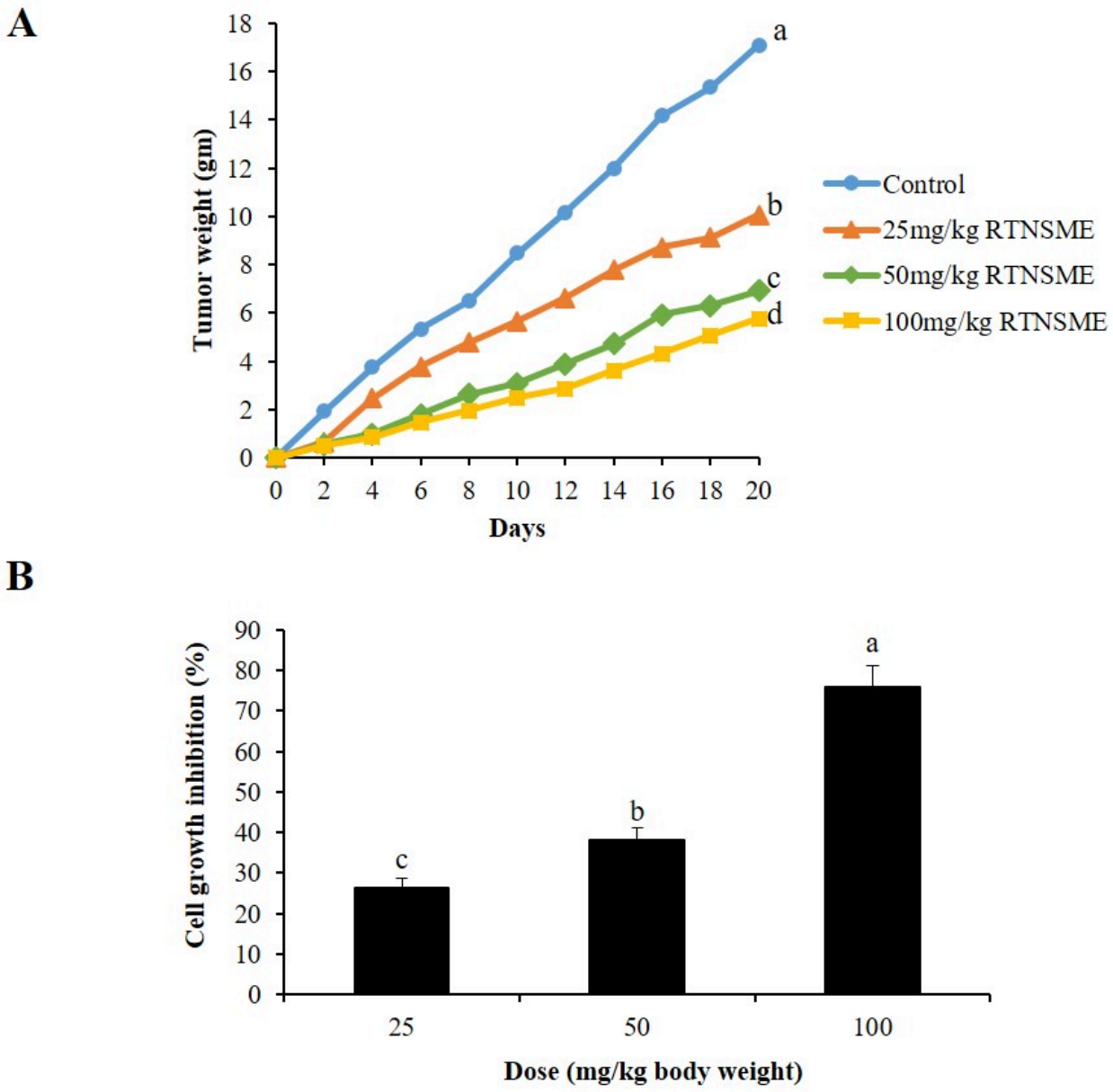

Figure 1

Effects of RTNSME on **(A)** Tumor weight of EAC bearing mice and **(B)** EAC cell growth inhibition. Results are shown as mean ± SD (standard deviation) (n=4). Mean with different lowercase letters are significantly different at $P < 0.05$ by Duncan's multiple-range test.

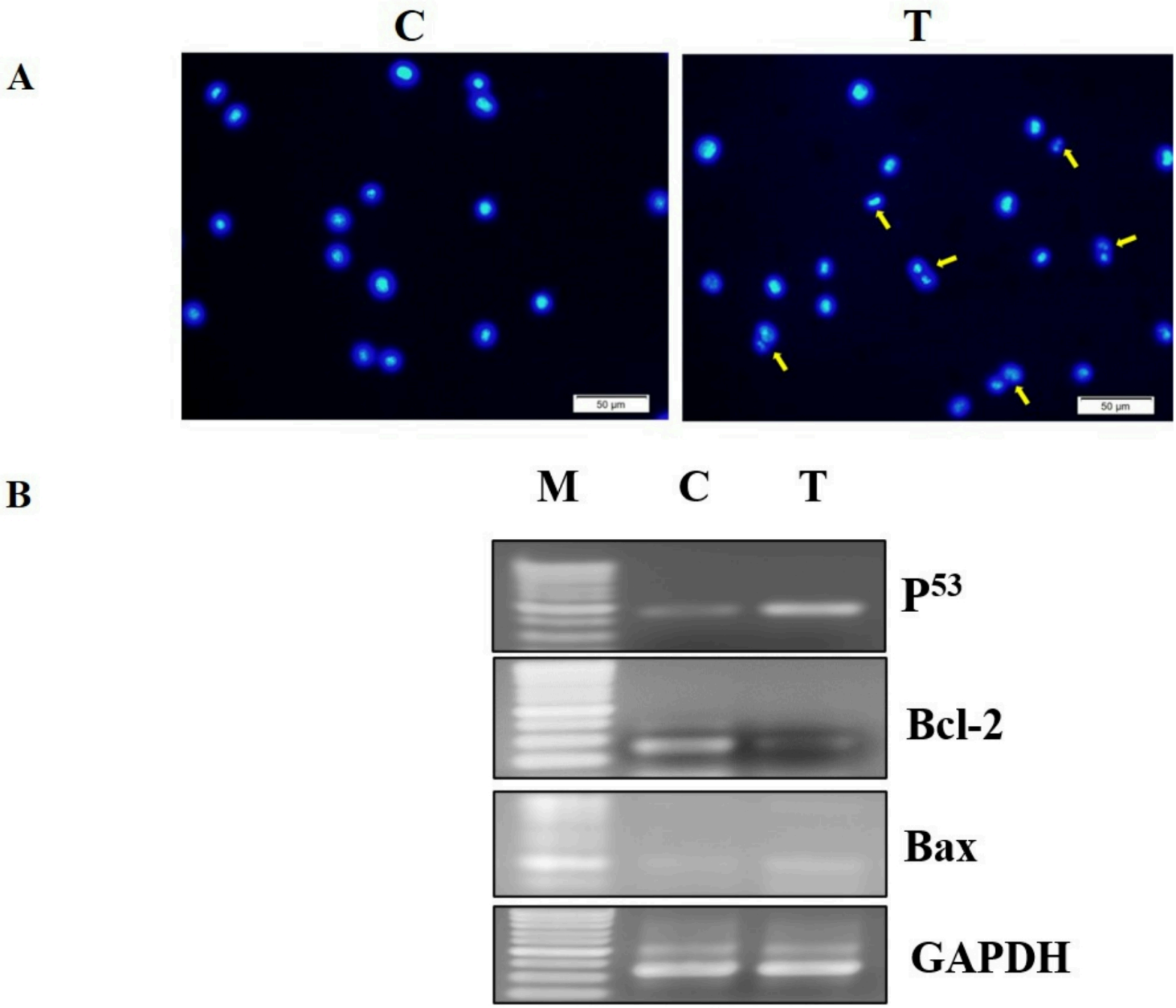

Figure 2

Induction of apoptosis in EAC cells treated with RTNSME. **(A)** DAPI staining of EAC cells treated with RTNSME followed by fluorescence microscopic analysis of cells. **(B)** Expression of P53, Bax and Bcl-2 genes in EAC cells treated with RTNSME. UV-trans illuminator visualizations of P53, Bcl-2, Bax and GAPDH. Here, M: Marker, C: EAC cells and T: EAC cells treated with RTNSME.

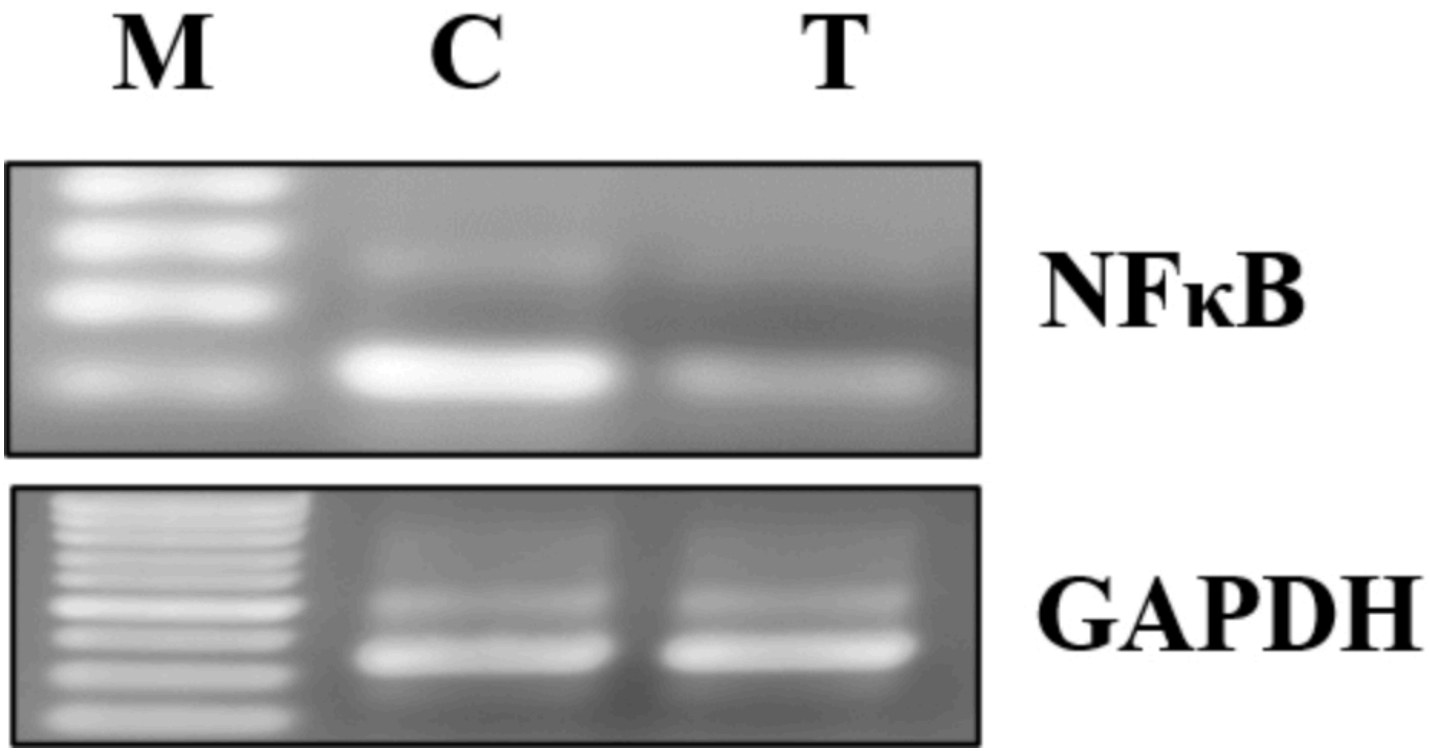

Figure 3

Inactivation of NF-κB gene expression in EAC cells treated with RTNSME. UV-trans illuminator visualizations of NF-κB and GAPDH. Here, M: Marker, C: EAC cells and T: EAC cells treated with RTNSME.

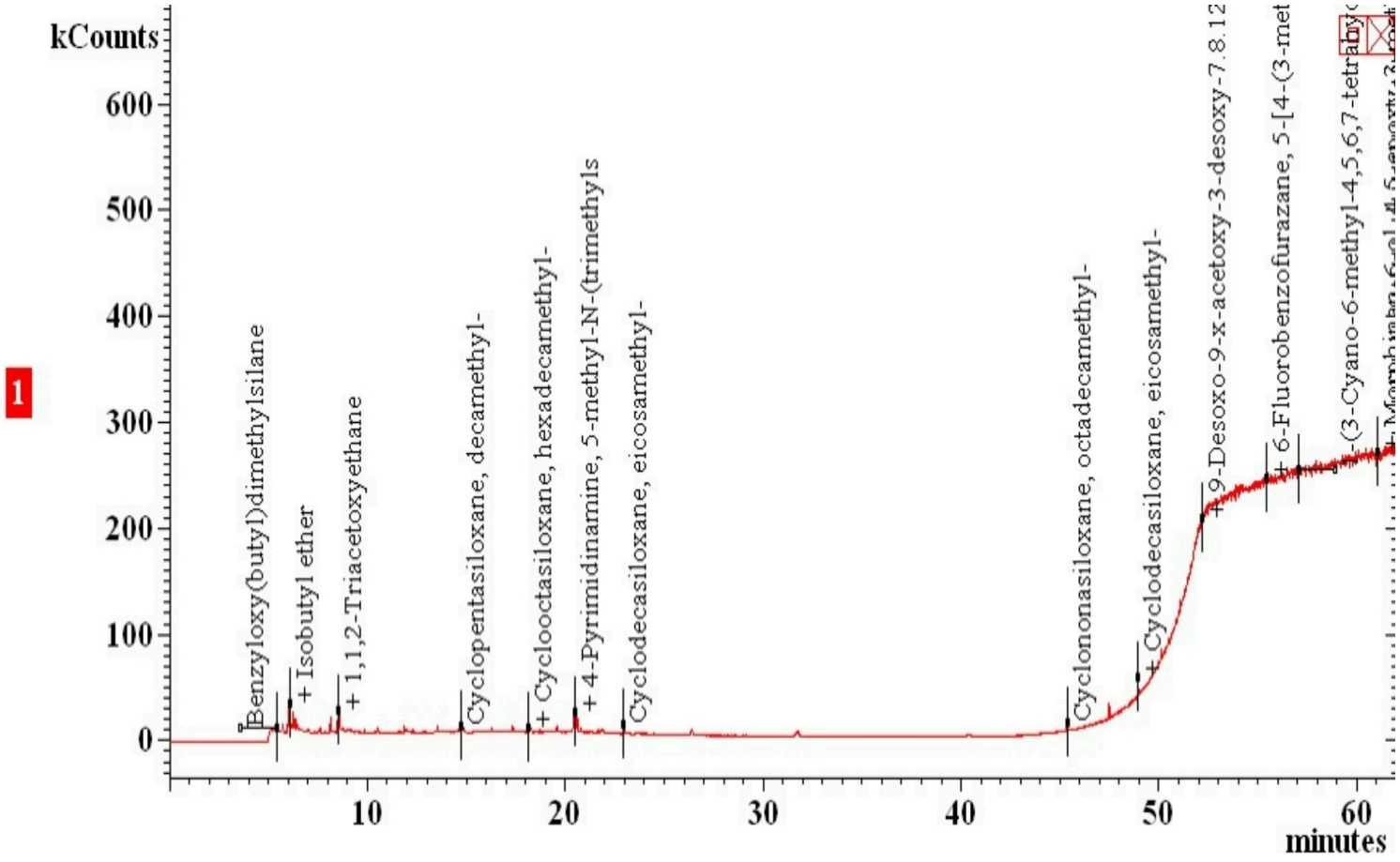

Figure 4

GC/MS chromatogram of RTNSME.

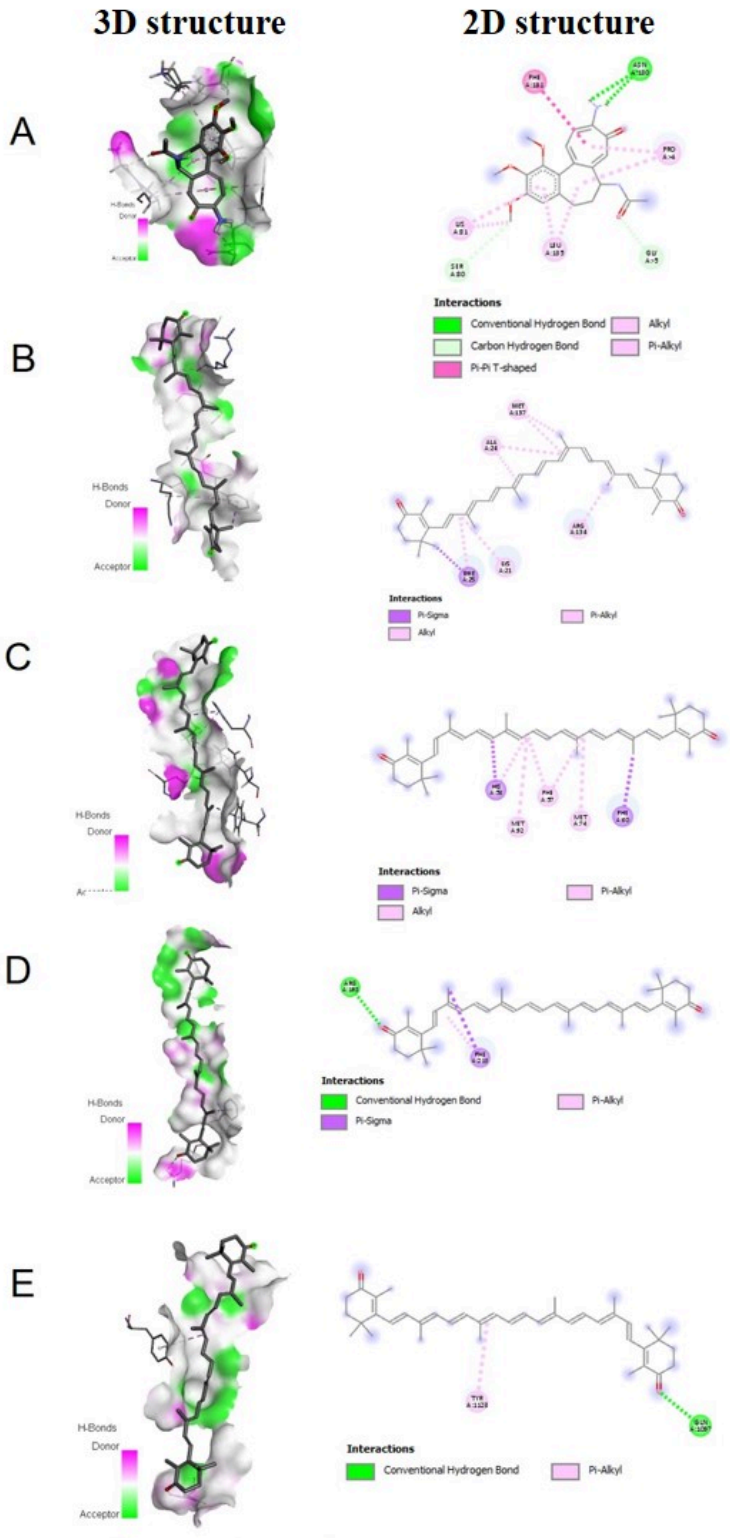

Figure 5

Binding affinity between Dipyridamole, Colchiceinamide, and Canthaxanthin with different proteins. **(A)** Represents binding of Colchiceinamide with BCL-2. While **(B)**, **(C)**, **(D)** and **(E)** represents interaction between Canthaxanthin with BAX, BCL2, p53, and NFkB, respectively.